

Bessel vortices in spin-1 Bose-Einstein condensates with Zeeman splitting and spin-orbit coupling

Huan-Bo Luo(罗焕波), Xin-Feng Zhang(张鑫锋), Runhua Li(李润华), Yongyao Li(黎永耀), and Bin Liu(刘彬)
Citation: Chin. Phys. B, 2024, 33 (**10**): 100304. DOI: 10.1088/1674-1056/ad6424
Journal homepage: http://cpb.iphy.ac.cn; http://iopscience.iop.org/cpb

What follows is a list of articles you may be interested in

Nonlinear modes coupling of trapped spin-orbit coupled spin-1 Bose-Einstein condensates

Jie Wang(王杰), Jun-Cheng Liang(梁俊成), Zi-Fa Yu(鱼自发), An-Qing Zhang(张安庆),Ai-Xia Zhang(张爱霞), and Ju-Kui Xue(薛具奎)
Chin. Phys. B, 2023, 32 (**9**): 090305. DOI: 10.1088/1674-1056/accd53

Electrical manipulation of a hole ‘spin’-orbit qubit in nanowire quantum dot: The nontrivial magnetic field effects

Rui Li(李睿) and Hang Zhang(张航)
Chin. Phys. B, 2023, 32 (**3**): 030308. DOI: 10.1088/1674-1056/ac873b

Spin-orbit coupling adjusting topological superfluid of mass-imbalanced Fermi gas

Jian Feng(冯鉴), Wei-Wei Zhang(张伟伟), Liang-Wei Lin(林良伟), Qi-Peng Cai(蔡启鹏), Yi-Cai Zhang(张义财), Sheng-Can Ma(马胜灿), and Chao-Fei Liu(刘超飞)
Chin. Phys. B, 2022, 31 (**9**): 090305. DOI: 10.1088/1674-1056/ac6860

Gap solitons of spin-orbit-coupled Bose-Einstein condensates in $\mathcal{PT}$ periodic potential

S Wang(王双), Y H Liu(刘元慧), and T F Xu(徐天赋)
Chin. Phys. B, 2022, 31 (**7**): 070306. DOI: 10.1088/1674-1056/ac538e

Anderson localization of a spin-orbit coupled Bose-Einstein condensate in disorder potential

Huan Zhang(张欢), Sheng Liu(刘胜), and Yongsheng Zhang(张永生)
Chin. Phys. B, 2022, 31 (**7**): 070305. DOI: 10.1088/1674-1056/ac538d

---

Bessel vortices in spin-1 Bose–Einstein condensates with Zeeman splitting and spin–orbit coupling

Huan-Bo Luo(罗焕波)[1,2], Xin-Feng Zhang(张鑫锋)[2], Runhua Li(李润华)[1], Yongyao Li(黎永耀)[2], and Bin Liu(刘彬)[2,†]

[1] *Department of Physics, South China University of Technology, Guangzhou* 510640, *China*
[2] *School of Physics and Optoelectronic Engineering, Foshan University, Foshan* 528000, *China*

(Received 14 June 2024; revised manuscript received 16 July 2024; accepted manuscript online 17 July 2024)

We investigate the ground states of spin–orbit coupled spin-1 Bose–Einstein condensates in the presence of Zeeman splitting. By introducing the generalized momentum operator, the linear version of the system is solved exactly, yielding a set of Bessel vortices. Additionally, based on linear solution and using variational approximation, the solutions for the full nonlinear system and their ground state phase diagrams are derived, including the vortex states with quantum numbers $m = 0$, 1, as well as mixed states. In this work, mixed states in spin-1 spin–orbit coupling (SOC) BEC are interpreted for the first time as weighted superpositions of three vortex states. Furthermore, the results also indicate that under strong Zeeman splitting, the system cannot form localized states. The variational solutions align well with numerical simulations, showing stable evolution and meeting the criteria for long-term observation in experiments.

Keywords: spin–orbit coupling, Bessel vortices, variational method

PACS: 03.75.Lm, 71.70.Ej, 75.70.Tj **DOI:** 10.1088/1674-1056/ad6424

1. Introduction

Bose–Einstein condensates (BECs) of atoms serve as versatile platforms for simulating a wide range of phenomena drawn from condensed-matter physics.[1–25] Among these phenomena, the spin–orbit coupling (SOC) plays a basic role in spin Hall effects,[26] topological insulators,[27] spintronic devices,[28] and more.[29–36] The experimental achievement of two-dimensional (2D) SOC[37] in spin-1/2 BECs is indeed a milestone, similar to its counterpart in one-dimensional (1D) case.[38] Recently, three-dimensional (3D) SOC in quantum gas has also been achieved experimentally.[39] Additionally, many schemes have been proposed.[40,41] The Gross–Pitaevskii equations (GPEs) are widely applied in studying the stationary state and dynamic behaviors of SOC BECs.[42] The diverse ground-state phase diagram of SOC spin-1/2 BECs, apart from including stripe, plane-wave, and zero-momentum phases,[43,44] also encompasses vortex states,[45–52] etc. In addition to ground states, solitons arising from the intrinsic nonlinear effects of SOC BECs have also been extensively studied and reported.[53–74]

In addition to spin-1/2, understanding the effect of spin-1 SOC in 2D BEC is also an active topic.[75] The spin-1 2D BEC system with SOC can support not only plane-wave and standing-wave phases,[76] but also vortex states,[77,78] and these vortex states have recently been proven to be Bessel vortices.[79] Furthermore, besides the equilibrium mode, the collective excitation modes of this system have also been reported recently.[80] In a spin-1/2 SOC BEC, in addition to the vortex state, another typical ground state is the mixed state. However, the mixed state has not been identified and explained well in spin-1 systems. Therefore, obtaining the complete ground state phase diagram for 2D spin-1 SOC BEC is essential for a comprehensive understanding of the entire system.

Recently, the gap solitons and the dynamics of bright solitons in SOC systems with Zeeman splitting have been studied.[81,82] However, the transition between the higher-order vortex state and the ground state is rarely studied. In our settings, under the action of Zeeman splitting added to the SOC system, higher-order vortex states can become the ground state. In this article, we will investigate the ground state of spin-1 SOC BEC with Zeeman splitting. In the linear case, by introducing the generalized momentum operator, the system can be exactly solved even in the presence of Zeeman splitting, with the solution being a set of Bessel vortices. In the nonlinear case, we construct a variational ansatz based on truncated linear solutions. The variational parameters are determined using the principle of minimum energy. Finally, by analyzing each variational parameter, we can obtain a complete ground state phase diagram. Under strong attractive interactions, the ground state of the system will transition from a vortex state to a mixed state. All variational results are in good agreement with the numerical results, and the stability of these ground states has been checked.

The rest of this paper is structured as follows. In Section 2, the theoretical model is introduced. In Section 3, the linear solution is constructed by means of Bessel function. Based on the linear vortex solutions, the nonlinear solution

†Corresponding author. E-mail: binliu@fosu.edu.cn

© 2024 Chinese Physical Society and IOP Publishing Ltd

is constructed by means of the variational approximation in Section 4. The vortex state and mixed state obtained through variational methods are discussed in Sections 5 and 6, respectively. Finally, the main results of the paper are summarized in Section 7.

2. Model and its reductions

We consider a quasi-(2D) spin-1 ^{7}Li BEC with Rashba-type spin–orbit coupling in the Zeeman field. The spinor wave function, $\Psi = (\Psi_1, \Psi_0, \Psi_{-1})^{\mathrm{T}}$, of this system can be governed by Gross–Pitaevskii (GP) equations in the dimensionless form

$$\mathrm{i}\partial_t \Psi = \left[-\frac{1}{2}\nabla_\perp^2 + V_{\mathrm{SO}} + k_z F_z - c_0 n - c_2 \boldsymbol{S}\cdot\boldsymbol{F}\right]\Psi, \tag{1}$$

where the spin–orbit (SO) coupling is chosen as $V_{\mathrm{SO}} = \mathrm{i}F_y\partial_x - \mathrm{i}F_x\partial_y$ and $\boldsymbol{F} = (F_x, F_y, F_z)$ is a vector of spin-1 matrices with

$$F_x = \frac{1}{\sqrt{2}}\begin{pmatrix} 0 & 1 & 0 \\ 1 & 0 & 1 \\ 0 & 1 & 0 \end{pmatrix}, \quad F_y = \frac{1}{\sqrt{2}}\begin{pmatrix} 0 & -\mathrm{i} & 0 \\ \mathrm{i} & 0 & -\mathrm{i} \\ 0 & \mathrm{i} & 0 \end{pmatrix},$$
$$F_z = \begin{pmatrix} 1 & 0 & 0 \\ 0 & 0 & 0 \\ 0 & 0 & -1 \end{pmatrix}. \tag{2}$$

The characteristic length, energy, and time are defined by $l = 2\ \mu\mathrm{m}$, $\varepsilon = \hbar^2/(ml^2) = 2.4\times10^{-31}$ J and $\tau = \hbar/\varepsilon = 0.44$ ms, where $m = 1.16\times10^{-26}$ kg is the mass of ^{7}Li. The coefficients $c_0 > 0$ and $c_2 > 0$ are the strengths of the particle-attraction and spin-attraction contact interactions, respectively. k_z represents the strength of the linear Zeeman effect. $n = \Psi^\dagger\Psi$ is the particle density and $\boldsymbol{S} = \Psi^\dagger\boldsymbol{F}\Psi$ is the local spin vector. Here, $c_0 = 1$ is fixed by means of rescaling. Thus, equation (1) includes only two free parameters k_z and c_2. In the absence of the Zeeman field in z direction, i.e., $k_z = 0$, equation (1) reduces to the case of Ref. [79], in which the vortex ground-state phase transition between the stationary vortex solutions, stability, and the unit Bloch vector textures were discussed. In this study, we will provide a detailed description of the vortex states and mixed states for the SOC spin-1 BECs in the presence of the Zeeman splitting.

Stationary solutions of Eq. (1) with chemical potential μ have the form

$$\Psi(x,y,t) = \psi(x,y)\exp(-\mathrm{i}\mu t), \tag{3}$$

where the stationary functions $\psi(x,y) = (\psi_1, \psi_0, \psi_{-1})^{\mathrm{T}}$. Furthermore, equation (1) can support vortex solutions given by

$$\begin{aligned} \psi_1(x,y) &= \mathrm{e}^{-\mathrm{i}(m+1)\theta}R_1(r), \\ \psi_0(x,y) &= \mathrm{e}^{-\mathrm{i}m\theta}R_0(r), \\ \psi_{-1}(x,y) &= \mathrm{e}^{-\mathrm{i}(m-1)\theta}R_{-1}(r), \end{aligned} \tag{4}$$

where (r,θ) are the polar coordinates and $R_{0,\pm1}(r)$ are three radial wave functions. m serves as a quantum number to index the vortex state. In the following, we will seek vortex solutions with the from of Eq. (4) form in both linear and nonlinear cases.

3. Exact vortex states of the linear version

The linear version of Eq. (1) can be considered as a special case where $c_0 = 0$ and $c_2 = 0$. By substituting Eq. (3) into the linear version of Eq. (1), we can obtain the stationary Schrödinger equation, i.e., $\hat{H}\psi = \mu\psi$, where the Hamiltonian $\hat{H}$ has the form

$$\hat{H} = -\nabla_\perp^2/2 + \mathrm{i}(F_y\partial_x - F_x\partial_y) + k_z F_z. \tag{5}$$

Solving this equation directly can be challenging, so we introduce a generalized momentum operator $\hat{P}$, which is defined by

$$\hat{P} = \mathrm{i}F_x\partial_y - \mathrm{i}F_y\partial_x - k_z F_z. \tag{6}$$

It is easy to check the Hamiltonian $\hat{H}$ and the generalized momentum operator $\hat{P}$ commute, i.e., $[\hat{H},\hat{P}] = 0$, which indicates that $\hat{H}$ and $\hat{P}$ share the same eigenstates. By solving the eigenvalue equation $\hat{P}\psi = k\psi$ with real k, we can obtain a set of eigenstates in the form (4) with

$$\begin{aligned} R_1 &= (k-k_z)\mathrm{J}_{m+1}(k_r r), \\ R_0 &= \sqrt{2}k_r\mathrm{J}_m(k_r r), \\ R_{-1} &= (k+k_z)\mathrm{J}_{m-1}(k_r r), \end{aligned} \tag{7}$$

where J_m denotes the Bessel function of the first kind with integer number m. k_r is the radial momentum and k_z can be considered as momentum in z component. Thus the total momentum should satisfy $k = \sqrt{k_r^2 + k_z^2}$. The solution (4) with Eq. (7) presents a set of the Bessel vortices with winding numbers $-(m+1)$, $-m$, and $-(m-1)$ in the ψ_1, ψ_0, and ψ_{-1} components, respectively. The similar exact solutions of the SO coupled binary linearlized GP equations were recently reported in Refs. [59,79,83].

The state given by Eq. (4) with Eq. (7) is also the eigenstate of $\hat{H}$, with the respective chemical potential

$$\mu(k) = \frac{k^2}{2} - k - \frac{k_z^2}{2}. \tag{8}$$

It includes the kinetic energy, SO-coupling energy and the energy induced by the Zeeman splitting. The chemical potential is a quadratic function of k, and always possesses a minimum value. Depending on the range of the total momentum k determined by k_z (i.e., $k = \sqrt{k_r^2 + k_z^2} \geq k_z$), we analyze the minimum values of the chemical potential in different cases. For $0 \leq k_z < 1$, the chemical potential reaches its minimum value $\mu_{\min} = -\left(1 + k_z^2\right)/2$ at $k = 1$, where the radial momentum is given by $k_r = \sqrt{k^2 - k_z^2} = \sqrt{1 - k_z^2}$. In the case of $k_z \geq 1$, the chemical potential achieves its minimum value $\mu_{\min} = -k_z$ at

$k = k_z$ with $k_r = 0$. The summary of the distribution of the minimum values of the chemical potential is as follows:

$$\mu_{\min} = \begin{cases} -\left(1+k_z^2\right)/2, & 0 \le k_z < 1, \\ -k_z, & k_z \ge 1. \end{cases} \tag{9}$$

The analysis above suggests that $k_z = 1$ is a critical point for a phase transition, wherein the ground state of the system transitions from vortex state to a uniform state. The uniform state can only exist in the case $m = 1$ with $\psi_1 = \psi_0 = 0$ and $\psi_{-1} = 1$. Note that all the vortex states are degenerate with respect to the excitation number m, but μ, given by Eq. (8), does not depend on m.

The linear Bessel vortices indicate that particles propagate radially with momentum k_r. Naturally, the norm integral (number of particles) for this linear state (7) in the free space diverges, which means that such states require an infinite number of particles and therefore cannot be realized in real world. As shown below, taking into account the attractive nonlinearity in Eq. (1) makes it possible to form localized state with a finite number of particles.

4. Variational method for ground state in nonlinear system

In the nonlinear case, we will employ both variational approximation (VA) and imaginary-time evolution method to solve the system simultaneously.

The attractive nonlinearity chops off the slowly decaying tails of the Bessel wave function, which make its integral norm diverging. To take this effect into account in the framework of the VA, we adopt an ansatz based on wave functions (4) and (7), multiplied by truncation factor $A\mathrm{sech}(ar)$, with amplitude A and inverse width a

$$\begin{aligned} \psi_1 &= (k-k_z)A\mathrm{sech}(ar)\sum_{m=-M}^{M} b_m \mathrm{e}^{-\mathrm{i}(m+1)\theta}\mathrm{J}_{m+1}(k_r r), \\ \psi_0 &= \sqrt{2}k_r A\mathrm{sech}(ar)\sum_{m=-M}^{M} b_m \mathrm{e}^{-\mathrm{i}m\theta}\mathrm{J}_{m}(k_r r), \\ \psi_{-1} &= (k+k_z)A\mathrm{sech}(ar)\sum_{m=-M}^{M} b_m \mathrm{e}^{-\mathrm{i}(m-1)\theta}\mathrm{J}_{m-1}(k_r r), \end{aligned} \tag{10}$$

where b_m represents the weight of the eigenstate in the superposition state with quantum number m, and it satisfies the condition that $\sum_{m=-M}^{M} b_m^2 = 1$. Here $M = 1$ is an empirical choice, thus there are only three weights, i.e., b_{-1}, b_0, and b_1. Similar truncation function $A\mathrm{sech}(ar)$ has already been applied in SO coupled systems in the absence of Zeeman splitting. The total momentum still satisfies $k = \sqrt{k_r^2 + k_z^2}$. The normalization coefficient A can be determined, as a function of a, b_{-1}, b_0, b_1, and k_r, by imposing the normalization condition, $\langle\psi|\psi\rangle = 1$.

In order to determine the parameters a, b_{-1}, b_0, b_1, and k_r, we need to minimize the total energy

$$E = \frac{1}{2}\iint \left[-\psi^{\dagger}\nabla_{\perp}^2\psi + c_0 n^2 + c_2 n^2 |\boldsymbol{S}|^2 + 2\psi^{\dagger}\left(\mathrm{i}F_y\partial_x - \mathrm{i}F_x\partial_y + k_z F_z\right)\psi\right]\mathrm{d}x\mathrm{d}y. \tag{11}$$

The specific expression for the total energy E can be obtained by substituting Eq. (10) into Eq. (11). The minimum energy value E and the corresponding variational parameters $(a, b_{-1}, b_0, b_1, k_r)$ can be numerically obtained by means of the simplex search method.[84]

Based on the distribution characteristics of variational parameters in the (k_z, c_2) plane, the phase diagram of the system's ground state is summarized in Fig. 1. We can find that the localized ground states of the system mainly include vortex states with quantum number $m = \pm 1$, and mixed states. Specifically, when both k_z and c_2 are small, the ground state of the system is a vortex state with $m = 0$, as indicated by the blue region in Fig. 1. However, when k_z remains small and c_2 increases, the ground state of the system becomes a mixed state, as illustrated by the green region in Fig. 1. When the Zeeman splitting strength is within a certain range, approximately $0.4 < k_z < 1.0$, the ground state of the system is a vortex state with $m = 1$, corresponding to the yellow region in Fig. 1. Furthermore, for strong Zeeman splitting k_z, the system will be unable to form localized ground states. In conclusion, we considered the limit of $k_z \to 0$, where the symmetric SOC term dominates, indicating a ground state that respects both spin symmetry and spatial rotational symmetry (vortex state with $m = 0$). In the limit of very large k_z, i.e., $k_z \ge 1$, only the Zeeman term takes effect, indicating that the ground state should be populated in ψ_{-1} and uniformly distributed in real space. In the middle range, the ground state is determined by the interplay of these two terms, resulting in a vortex state with $m = 1$. In the following, we will discuss in detail the characteristics of vortex states and mixed states by fixing $c_2 = 0$ and $c_2 = 0.3$, respectively.

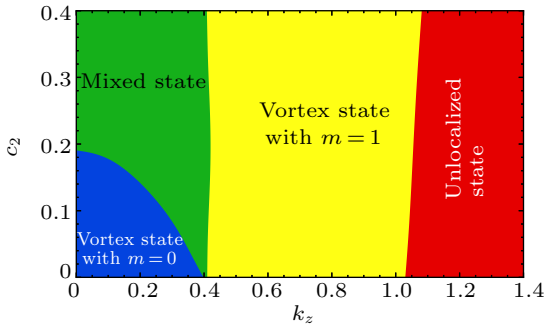


Fig. 1. Diagram of the ground state in (k_z, c_2) plane.

5. Vortex states as ground states in the absence of spin interactions

Firstly, we consider the ground state of the system in the absence of spin–spin interactions. Figures 2(a)–2(d) illustrate the dependence of variational parameters on k_z at $c_2 = 0$. In Fig. 2(a), it is evident that, for $k_z < 0.4$, the weights $b_0 = 1$, and

$b_1 = b_{-1} = 0$. This signifies that the system's ground state corresponds to a vortex state with $m = 0$. Conversely, for $k_z > 0.4$, the weights become $b_1 = 1$, and $b_0 = b_{-1} = 0$. In this region, the ground state of the system is also a vortex state, but with a quantum number of $m = 1$. Therefore, $k_z = 0.4$ is the ground state phase transition point. From Figs. 2(b)–2(d), it can be observed that for $k_z > 1.05$, a, A, and k_r all become 0. The result implies that the uniform state cannot form localized states in free space.

To validate the accuracy of the variational results, we numerically solved Eq. (1) using the imaginary-time evolution method. By setting $c_2 = 0$, we obtained the system's ground states for Zeeman field strengths at $k_z = 0$ and 0.7, respectively. The wavefunctions for a three-component system can be expressed as

$$\psi_j = |\psi_j| \exp(\mathrm{i}\Theta_j), \quad j = 0, \pm 1, \tag{12}$$

where $|\psi_j|$ and Θ_j are amplitude and phase of the wavefunction. The distributions of the amplitude and phase for $k_z = 0$ and 0.7 are shown in Figs. 3(a1)–3(a3) and 3(c1)–3(c3). However, the system cannot support a localized ground state under strong Zeeman splitting ($k_z > 1.05$), and such phenomenon also observed in spin-1/2 systems.[48]

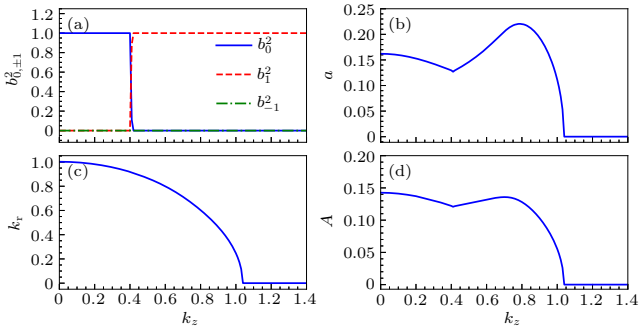


Fig. 2. (a) Weights $b_{0,\pm1}$, (b) inverse width a, (c) radial momentum k_r, and (d) normalization coefficient A as a function of strength of Zeeman splitting k_z at $c_2 = 0$.

To compare the variational method with numerical method, the distributions of the amplitude and phase for $k_z = 0$ and 0.7 obtained through the variational method are displayed in Figs. 3(b1)–3(b3) and 3(d1)–3(d3). Here the variational parameters in Eq. (10) calculated by variational method are $a = 0.1621$, $b_0 = 1$, $b_1 = b_{-1} = 0$, $k_r = 1.0023$, $A = 0.1426$ and $a = 0.2054$, $b_1 = 1$, $b_0 = b_{-1} = 0$, $k_r = 0.7129$, $A = 0.1358$ for $k_z = 0$ and $k_z = 0.7$, respectively.

Overall, the results obtained from the variational method are essentially consistent with those from numerical method, including both the amplitude distributions and phase distributions. Therefore, below we will only use the variational results to analyze the characteristics of the solutions. From Figs. 3(b1)–3(b3), it can be observed that for $k_z = 0$, the distributions of Θ_1, Θ_0, and Θ_{-1} have winding numbers of 1, 0, and -1, respectively. This implies that the ground state of the system corresponds to a vortex state with $m = 0$. Furthermore, the distributions of the amplitudes $|\psi_1|$, $|\psi_0|$, and $|\psi_{-1}|$ exhibit concentric ring patterns for each. Similarly, from Figs. 3(d1)–3(d3), it can be seen that for $k_z = 0.7$, the distributions of Θ_1, Θ_0, and Θ_{-1} have winding numbers of 2, 1, and 0, respectively. This indicates that the ground state of the system corresponds to a vortex state with $m = 1$. the distributions of the amplitudes $|\psi_1|$, $|\psi_0|$, and $|\psi_{-1}|$ also exhibit concentric ring patterns for each. Additionally, we find that under the action of a stronger Zeeman field ($k_z = 0.7$), the atoms are predominantly populated in the ψ_{-1} component, followed by the ψ_0 component, with the least population in the ψ_{-1} component.

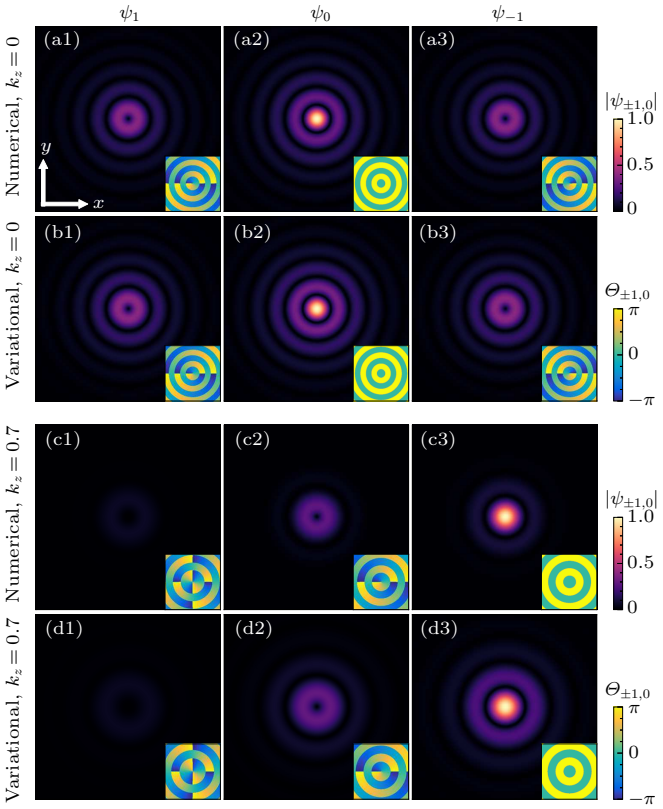


Fig. 3. The distributions of the amplitude and phase of wave functions obtained by variational and numerical methods. The numerical results correspond to parameters [(a1)–(a3)] $k_z = 0$, $c_2 = 0$, and [(c1)–(c3)] $k_z = 0.7$, $c_2 = 0$, while the variational results correspond to parameters [(b1)–(b3)] $k_z = 0$, $c_2 = 0$, and [(d1)–(d3)] $k_z = 0.7$, $c_2 = 0$. In each figure the bottom right corner depicts the phase distribution of the wave function.

Figure 4 compares the profiles of the wave function at $y = 0$ obtained through numerical method and the variational method for two different sets of parameters $k_z = 0$ and $k_z = 0.7$. Note that, as per Eq. (10), the imaginary component of the wave function is absent, i.e., $\mathrm{Im}(\psi_{0,\pm1}) = 0$. One can see that for $k_z = 0$, numerical wave functions are nearly identical to the variational counterparts, while for $k_z = 0.7$, there is a slight mismatch at peaks and valleys as shown in Fig. 4(f). Since the variational method is semi-analytical, mismatch always exists. Even the mismatch in Fig. 4(f) is within the tolerance range. Providing more complex ansatz may reduce mis-

match. These results indicate that the variational method based on the ansatz (10) exhibits high accuracy and reliability, with the accuracy increasing as k_z decreases.

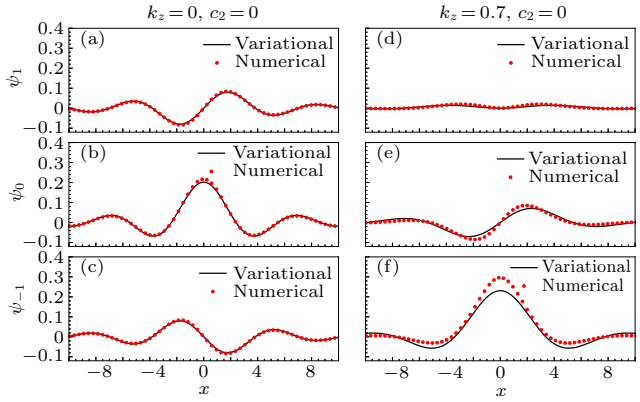


Fig. 4. The wave function profiles at $y = 0$ are depicted, with the solid line representing the variational result and the dashed line representing the numerical result. The wave functions [(a)–(c)] correspond to ψ_1, ψ_0, and ψ_{-1} under the parameters $k_z = 0.0$ and $c_2 = 0.0$, while panels (d)–(f) correspond to the same wave functions under $k_z = 0.7$ and $c_2 = 0.0$.

6. Emergence of mixed states in the presence of spin interactions

In the previous section, we mainly discussed the ground state of the system in the absence of spin and spin interactions, i.e., when $c_2 = 0$, and demonstrated that the ground state corresponds to vortex states with $m = 0$ or 1. In the case of $c_2 \neq 0$, mixed states rather than vortex states can also serve as the ground state of the system. Here, we choose $c_2 = 0.3$ as a typical example to analyze the ground state of the system under different values of k_z.

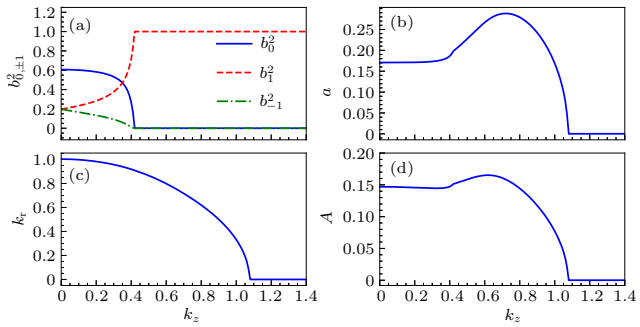


Fig. 5. (a) Weights $b_{0,\pm1}$, (b) inverse width a, (c) radial momentum k_r, and (d) normalization coefficient A as a function of strength of Zeeman splitting k_z at $c_2 = 0.3$.

The variational parameters in the ansatz (10) for $c_2 = 0.3$ are presented in Fig. 5. We can find that the weights b_0, b_1, and b_{-1} are all non-zero for $k_z < 0.42$, indicating that under this condition, the ground state of the system is a mixed state. Specifically, at $k_z = 0$, $b_1^2 = b_{-1}^2 \approx 0.2$, and $b_0^2 \approx 0.6$. This indicates that in the mixed state, the vortex states with $m = 1$ and $m = -1$ have equal weights, while the vortex state with $m = 0$ predominates. As k_z increases, b_1 and b_0 gradually decrease, while b_1 increases. Until $k_z = 0.42$, b_{-1} and b_0 approach 0, and b_1 becomes 1. This implies that $k_z = 0.42$ is a ground state phase transition point, where the system's ground state transitions from a mixed state to a vortex state with $m = 1$.

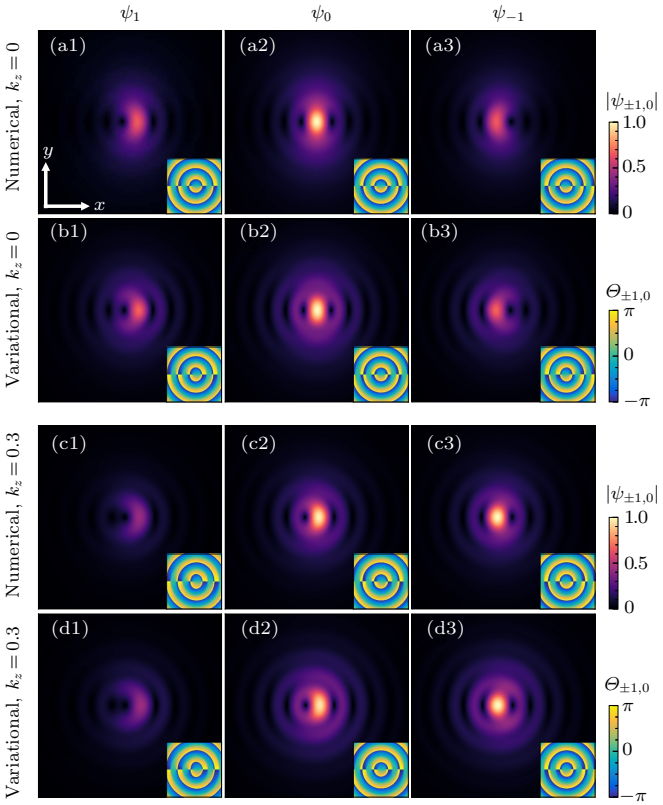


Fig. 6. The distributions of the amplitude and phase of wave functions obtained by variational and numerical methods. The numerical results correspond to parameters [(a1)–(a3)] $k_z = 0$, $c_2 = 0.3$, and [(c1)–(c3)] $k_z = 0.3$, $c_2 = 0.3$, while the variational results correspond to parameters [(b1)–(b3)] $k_z = 0$, $c_2 = 0.3$, and [(d1)–(d3)] $k_z = 0.3$, $c_2 = 0.3$. In each figure the bottom right corner depicts the phase distribution of the wave function.

As typical examples, the distributions of the amplitude and phase obtained through variational method for $k_z = 0$ and $k_z = 0.3$ are respectively shown in Figs. 6(b1)–6(b3) and 3(d1)–3(d3). Here the variational parameters in Eq. (10) calculated by variational method are $a = 0.1694$, $b_0 = 0.7815$, $b_1 = b_{-1} = 0.4412$, $k_r = 1.0034$, $A = 0.1464$ for $k_z = 0$, and $a = 0.1717$, $b_1 = 0.6111$, $b_0 = 0.7315$, $b_{-1} = 0.3024$, $k_r = 0.7129$, $A = 0.1440$ for $k_z = 0.3$. On the other hand, we also employed the imaginary time evolution method to determine the ground state of the system under the parameters $c_2 = 0.3$, $k_z = 0$, and $c_2 = 0.3$, $k_z = 0.3$. The corresponding distributions of the amplitude and phase are shown in Figs. 6(a1)–6(a3) and 6(c1)–6(c3). By comparing distributions of the amplitude and phase obtained through variational method and numerical method, we can see that these two patterns are very similar. By observing the distributions of amplitude, we can find that the rotational symmetry of a mixed state is broken compared to a vortex state. Additionally, we can also find that the phase of a vortex state changes gradually along the azimuthal direction, while in a mixed state, it changes gradually along the radial direction. In addition, we

can draw a conclusion that in the absence of Zeeman splitting ($k_z = 0$), the component density distributions of ψ_1 and ψ_{-1} are mirror symmetric about $x = 0$, i.e., $\psi_1(x, y) = \psi_{-1}(-x, y)$. This symmetry holds for both vortex states and mixed states, as shown in Figs. 3(a1)–3(a3) and 6(a1)–6(a3). However, in the presence of Zeeman splitting, this symmetry is broken.

Figure 7 compares the profiles of the wave function at $y = 0$ obtained through numerical method and the variational method for two different sets of parameters $k_z = 0$ and $k_z = 0.3$. Note that, as per Eq. (10), the imaginary component of the wave function is absent, i.e., $\mathrm{Im}(\psi_{0,\pm1}) = 0$. One can see that for both $k_z = 0$ and $k_z = 0.3$, numerical wave functions are nearly identical to the variational counterparts. This result implies that variational method also exhibit a considerable level of accuracy for solving mixed states. Furthermore, this also indicates that the ansatz we provided in Eq. (10) is reasonable, and mixed states are superpositions formed by three vortex states. It is relevant to mention that mixed states in spin-1 SOC BEC have already been reported in Ref. [77], but the composition of these mixed states has not been explained yet.

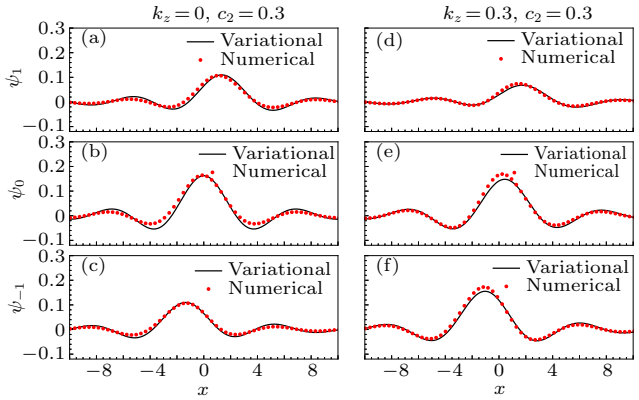


Fig. 7. The wave function profiles at $y = 0$ are depicted, with the solid line representing the variational result and the dashed line representing the numerical result. The wave functions [(a)–(c)] correspond to ψ_1, ψ_0, and ψ_{-1} under the parameters $k_z = 0.0$ and $c_2 = 0.3$, while [(d)–(f)] correspond to the same wave functions under $k_z = 0.3$ and $c_2 = 0.3$.

To confirm that the ground states identified by the above analyses are indeed stable modes, their stability was verified through real-time simulations of their perturbed evolution. White noise, with maximum intensity reaching 10% of the wave function's amplitude, was added to the ground-state wave functions. Subsequently, real-time evolution was applied to these perturbed wave functions. The results of numerical simulations, presented in Figs. 8, showcase a vortex state with parameters $k_z = 0.0$ and $c_2 = 0.0$, and a mixed state with parameters $k_z = 0.0$ and $c_2 = 0.3$. At $t = 0$, the wave functions exhibit numerous noise points. However, as time progresses, by $t = 200$, the noise points on the wave functions disappear. In the subsequent evolution, the phases of the wave functions rotate around the vortex centers, while the amplitude distribution remains unchanged. These results fully verify the stability of the ground states in all cases.

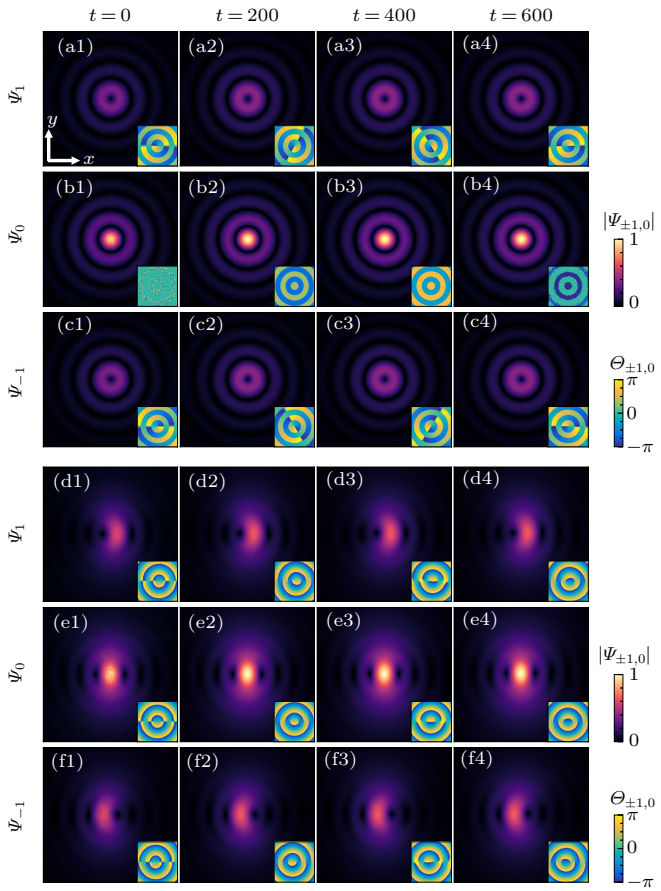


Fig. 8. Numerical evolution of the perturbed ground state, where panels (a1)–(a4), (b1)–(b4), and (c1)–(c4) correspond to vortex state with parameters $k_z = 0.0$ and $c_2 = 0.0$, while panels (d1)–(d4), (e1)–(e4), and (f1)–(f4) correspond to mixed state with parameters $k_z = 0.0$ and $c_2 = 0.3$. In each figure the bottom right corner depicts the phase distribution of the wave function. From left to right, each column corresponds to the wave-function density and phase distribution at evolution time $t = 0$ (initial state), $t = 200$, $t = 400$, and $t = 600$, respectively.

7. Conclusions

In summary, we investigated the ground state of vortex formation in spin-1 BECs under the combined effects of spin–orbit coupling and Zeeman splitting. The linear version of the system can be solved exactly by introducing the generalized momentum operator, resulting in a set of Bessel vortices. Additionally, based on these Bessel vortices and using variational approximation, we have derived solutions for the full nonlinear system. Through an analysis of the variational parameters, we have summarized the phase diagrams of the system under different c_2 and k_z parameters. These phases include vortex states with quantum numbers m equaling 0 and 1, as well as mixed states. It is worth noting that under strong Zeeman splitting, specifically when k_z approaches or exceeds 1, localized states cannot exist. Our results demonstrate that the variational solutions are in good agreement with numerical simulations and exhibit stable evolution, meeting the requirements for long-time observation in experiments.

Acknowledgements

Project supported by the Guangdong Basic and Applied Basic Research Foundation (Grant No. 2023A1515110198), the Natural Science Foundation of Guangdong Province, China (Grant Nos. 2024A1515030131 and 2021A1515010214), the National Natural Science Foundation of China (Grant Nos. 12274077, 11905032, and 12475014), the Research Fund of the Guangdong–Hong Kong–Macao Joint Laboratory for Intelligent Micro-Nano Optoelectronic Technology (Grant No. 2020B1212030010), and the Israel Science Foundation (Grant No. 1695/22).

References

[1] Hauke P, Cucchietti F M, Tagliacozzo L, Deutsch I and Lewenstein M 2012 *Rep. Prog. Phys.* **75** 082401
[2] Lewenstein M, Sanpera A and Ahufinger V 2012 *Ultracold Atoms in Optical Lattices: Simulating quantum many-body systems* (Oxford)
[3] Chen G H, Wang H C, Deng H M and Malomed B A 2024 *Chin. Phys. Lett.* **41** 020501
[4] Qin Y H, Wu Y, Zhao L C and Yang Z Y 2020 *Chin. Phys. B* **29** 020303
[5] Yang A W, Zhou J H, Liang X Q, Li G L, Liu B, Luo H B, Malomed B A and Li Y Y 2024 *New J. Phys.* **26** 053037
[6] Liu B, Cai X Y, Qin X ZH, Jiang X D, Xie J N, Malomed B A and Li Y Y 2023 *Phys. Rev. E* **108** 044210
[7] Li G L, Jiang X D, Liu B, Chen Zh P, Malomed B A and Li Y Y 2024 *Front. Phys.* **19** 22202
[8] Deng H M, Li J Q, Chen Zh P, Liu D, Jiang Ch Z, Kong C and Malomed B A 2024 *Phys. Rev. E* **109** 064201
[9] Wang Y, Guo L, Yi S and Shi T 2020 *Phys. Rev. Res.* **2** 043074
[10] Wang J, Liu X and Hu H 2021 *Chin. Phys. B* **30** 010306
[11] Liu B, Chen Y, Yang A, Cai X, Liu Y, Luo Z, Qin X, Jiang X, Li Y and Malomed B A 2022 *New J. Phys.* **24** 123026
[12] Zhang X M, Qin Y H, Ling L M and Zhao L C 2021 *Chin. Phys. Lett.* **39** 090201
[13] Zhu J Z and Huang G X 2023 *Chin. Phys. Lett.* **40** 100504
[14] Zhang X, Xu X, Zheng Y, Chen Z, Liu B, Huang C, Malomed B A and Li Y 2019 *Phys. Rev. Lett.* **123** 133901
[15] Liu B, Zhang H, Zhong R, Zhang X, Qin X, Huang C, Li Y and Malomed B A 2019 *Phys. Rev. A* **99** 053602
[16] Ding C C, Zhou Q, Xu S L, Triki H, Mirzazadeh M and Liu W 2023 *Chin. Phys. Lett.* **40** 040501
[17] Zhang Y L, Jia C Y and Liang Z X 2022 *Chin. Phys. Lett.* **39** 020501
[18] Guo M and Pfau T 2021 *Front. Phys.* **16** 32202
[19] Dong L and Kartashov Y V 2021 *Phys. Rev. Lett.* **126** 244101
[20] Luo Z, Pang W, Liu B, Li Y and Malomed B A 2021 *Front. Phys.* **16** 32201
[21] Wang J B, Pan J S and Cui X L 2020 *Chin. Phys. Lett.* **37** 076701
[22] Wang L X, Dai C Q, Wen L, Liu T, Jiang H F, Saito H, Zhang S G and Zhang X F 2018 *Phys. Rev. A* **97** 063607
[23] Li Y, Liu Y, Fan Z, Pang W, Fu S H and Malomed B A 2017 *Phys. Rev. A* **95** 063613
[24] Xu T F, Li W L, Li Z D and Zhang C 2018 *Chaos, Solitons and Fractals* **111** 62
[25] Wen L, Zhang X F, Hu A Y, Zhou J, Yu P, Xia L, Sun Q and Ji A C 2018 *Ann. Phys.* **390** 180
[26] Xiao D, Chang M C and Niu Q 2010 *Rev. Mod. Phys.* **82** 1959
[27] Hasan M Z and Kane C L 2010 *Rev. Mod. Phys.* **82** 3045
[28] Žutić I, Fabian J and Sarma S D 2004 *Rev. Mod. Phys.* **76** 323
[29] He J T, Fang B B and Lin J 2022 *Chin. Phys. Lett.* **39** 020301
[30] Li Z, Wang J Z and Fu L B 2013 *Chin. Phys. Lett.* **30** 010301
[31] Wang J, Liang J C, Yu Z F, Zhang A Q, Zhang A X and Xue J K 2023 *Chin. Phys. B* **32** 090305
[32] Zhu H, Yin S G and Liu W M 2022 *Chin. Phys. B* **31** 060305
[33] Zhu H, Yin S G and Liu W M 2022 *Chin. Phys. B* **31** 040306
[34] Li J, He T C, Bai J, Liu B and Wang H Y 2021 *Chin. Phys. B* **30** 030302
[35] Liu K Y, He H X, Wang C H, Chen Y Y and Zhang Y P 2022 *Phys. Rev. A* **105** 013323
[36] Lü H, Zhu S B, Qian J and Wang Y Z 2015 *Chin. Phys. B* **24** 090308
[37] Wu Z, Zhang L, Sun W, Xu X T, Wang B Z, Ji S C, Deng Y, Chen S, Liu X J and Pan J W 2016 *Science* **354** 83
[38] Lin Y J, Jiménez-García K and Spielman I B 2011 *Nature* **471** 83
[39] Wang Z Y, Cheng X C, Wang B Z, Zhang J Y, Lu Y H, Yi C R, Niu S, Deng Y, Liu X J, Chen S and Pan J W 2021 *Science* **372** 271
[40] Anderson B M, Juzeliūnas G, Galitski V M and Spieman I B 2012 *Phys. Rev. Lett.* **108** 235301
[41] Xiong L, Gong M, Fang Z X and Sun R 2023 *Chin. Phys. Lett.* **40** 127402
[42] Zhang Y, Mao L and Zhang C 2012 *Phys. Rev. Lett.* **108** 035302
[43] Luo H B, Malomed B A, Liu W M and Li L 2022 *Phys. Rev. A* **106** 063311
[44] Wang C, Gao C, Jian C M and Zhai H 2010 *Phys. Rev. Lett.* **105** 160403
[45] Kawakami T, Mizushima T and Machida K 2011 *Phys. Rev. A* **84** 011607
[46] Ramachandhran B, Opanchuk B, Liu X J, Pu H, Drummond P D and Hu H 2012 *Phys. Rev. A* **85** 023606
[47] Sakaguchi H, Li B and Malomed B A 2014 *Phys. Rev. E* **89** 032920
[48] Sakaguchi H, Sherman E Y and Malomed B A 2016 *Phys. Rev. E* **94** 032202
[49] Sakaguchi H and Li B 2013 *Phys. Rev. A* **87** 015602
[50] Luo H B, Malomed B A, Liu W M and Li L 2022 *Commun. Nonlinear Sci. Numer. Simul.* **115** 106769
[51] Zhu H, Yin S G and Liu W M 2022 *Chin. Phys. B* **31** 040306
[52] Luo H B, Li L, Malomed B A, Li Y and Liu B 2024 *Phys. Rev. A* **109** 013326
[53] Achilleos V, Frantzeskakis D J, Kevrekidis P G and Pelinovsky D E 2013 *Phys. Rev. Lett.* **110** 264101
[54] Chen X, Deng Z, Xu X, Li Sh, Fan Z, Chen Zh, Liu B and Li Y 2020 *Nonlinear Dyn.* **101** 569
[55] Salasnich L and Malomed B A 2013 *Phys. Rev. A* **87** 063625
[56] Kartashov Y V, Konotop V V and Abdullaev F Kh 2013 *Phys. Rev. Lett.* **111** 060402
[57] Salasnich L, Cardoso W B and Malomed B A 2014 *Phys. Rev. A* **90** 033629
[58] Lobanov V E, Kartashov Y V and Konotop V V 2014 *Phys. Rev. Lett.* **112** 180403
[59] Li Y, Liu Y, Fan Z, Pang W, Fu S and Malomed B A 2017 *Phys. Rev. A* **95** 063613
[60] Sakaguchi H and Malomed B A 2018 *Phys. Rev. A* **97** 013607
[61] Kartashov Y V, Torner L, Modugno M, Sherman E Ya, Malomed B A and Konotop V V 2020 *Phys. Rev. Res.* **2** 013036
[62] Zhang Y C, Zhou Z W, Malomed B A and Pu H 2015 *Phys. Rev. Lett.* **115** 253902
[63] Zhang H F, Chen F, Yu C C, Sun L H and Xu D H 2017 *Chin. Phys. B* **26** 080304
[64] Wang X, Tan R B, Du Z J, Zhao W Y, Zhang X F and Zhang S G 2014 *Chin. Phys. B* **23** 070308
[65] Ye Z J, Chen Y X, Zheng Y L, Chen X W and Liu B 2020 *Chaos, Solitons and Fractals* **130** 109418
[66] Li Y E and Xue J K 2016 *Chin. Phys. Lett.* **33** 100502
[67] Wang S, Liu Y H and Xu T F 2022 *Chin. Phys. B* **31** 070306
[68] Guo H, Qiu X, Ma Y, Jiang H F and Zhang X F 2021 *Chin. Phys. B* **30** 060310
[69] Xu Y, Zhang Y P and Wu B 2013 *Phys. Rev. A* **87** 013614
[70] Pang W, Deng H, Liu B, Xu J and Li Y 2018 *Appl. Sci.* **8** 1771
[71] Shamriz E, Chen Z P and Malomed B A 2020 *Commun. Nonlinear Sci. Numer. Simulat.* **91** 105412
[72] Liu B, Zhong R X, Chen Z P, Qin X Z, Zhong H H, Li Y Y and Malomed B A 2020 *New J. Phys.* **22** 043004
[73] Wen L, Liang Y, Zhou J, Yu P, Xia L, Niu L B and Zhang X F 2019 *Acta Phys. Sin.* **68** 080301 (in Chinese)
[74] Xu X X, Zhao F Y, Zhou Y G, Liu B, Jiang X D, Malomed B A and Li Y Y 2023 *Commun. Nonlinear Sci. Numer. Simulat.* **117** 106930
[75] He J T, Fang P P and Lin J 2022 *Chin. Phys. Lett.* **39** 020301
[76] Wen L, Sun Q, Wang H Q, Ji A C and Liu W M 2012 *Phys. Rev. A* **86** 043602
[77] Gautam S and Adhikari S K 2017 *Phys. Rev. A* **95** 013608
[78] Adhikari S K 2021 *Phys. Rev. A* **103** L011301
[79] Li J Z, Luo H B and Li L 2022 *Phys. Rev. A* **106** 063321
[80] Mithun T, Fritsch A R, Koutsokostas G N, Frantzeskakis D J, Spielman I B and Kevrekidis P G 2024 *Phys. Rev. A* **109** 023328
[81] Wen L, Liang Y, Zhou J, Yu P, Xia L, Niu L B and Zhang X F 2019 *Acta Phys. Sin.* **68** 080301 (in Chinese)
[82] Sakaguchi H and Malomed B A 2018 *Phys. Rev. A* **97** 013607
[83] Chen Z, Li Y and Malomed B A 2020 *Phys. Rev. Res.* **2** 033214
[84] Lagarias J C, Reeds J A, Wright M H and Wright P E 1998 *SIAM J. Optimiz.* **9** 112